NASA/TM—2002-211504 AIAA–2002–0827

Rayleigh Scattering Diagnostic for Measurement of Velocity and Density Fluctuation Spectra

Richard G. Seasholtz
Glenn Research Center, Cleveland, Ohio

Jayanta Panda
Ohio Aerospace Institute, Brook Park, Ohio

Kristie A. Elam
Akima Corporation, Cleveland, Ohio

April 2002

The NASA STI Program Office . . . in Profile

Since its founding, NASA has been dedicated to the advancement of aeronautics and space science. The NASA Scientific and Technical Information (STI) Program Office plays a key part in helping NASA maintain this important role.

The NASA STI Program Office is operated by Langley Research Center, the Lead Center for NASA's scientific and technical information. The NASA STI Program Office provides access to the NASA STI Database, the largest collection of aeronautical and space science STI in the world. The Program Office is also NASA's institutional mechanism for disseminating the results of its research and development activities. These results are published by NASA in the NASA STI Report Series, which includes the following report types:

- TECHNICAL PUBLICATION. Reports of completed research or a major significant phase of research that present the results of NASA programs and include extensive data or theoretical analysis. Includes compilations of significant scientific and technical data and information deemed to be of continuing reference value. NASA's counterpart of peer-reviewed formal professional papers but has less stringent limitations on manuscript length and extent of graphic presentations.

- TECHNICAL MEMORANDUM. Scientific and technical findings that are preliminary or of specialized interest, e.g., quick release reports, working papers, and bibliographies that contain minimal annotation. Does not contain extensive analysis.

- CONTRACTOR REPORT. Scientific and technical findings by NASA-sponsored contractors and grantees.

- CONFERENCE PUBLICATION. Collected papers from scientific and technical conferences, symposia, seminars, or other meetings sponsored or cosponsored by NASA.

- SPECIAL PUBLICATION. Scientific, technical, or historical information from NASA programs, projects, and missions, often concerned with subjects having substantial public interest.

- TECHNICAL TRANSLATION. English-language translations of foreign scientific and technical material pertinent to NASA's mission.

Specialized services that complement the STI Program Office's diverse offerings include creating custom thesauri, building customized data bases, organizing and publishing research results . . . even providing videos.

For more information about the NASA STI Program Office, see the following:

- Access the NASA STI Program Home Page at ***http://www.sti.nasa.gov***

- E-mail your question via the Internet to help@sti.nasa.gov

- Fax your question to the NASA Access Help Desk at 301–621–0134

- Telephone the NASA Access Help Desk at 301–621–0390

- Write to:
  NASA Access Help Desk
  NASA Center for AeroSpace Information
  7121 Standard Drive
  Hanover, MD 21076

NASA/TM—2002-211504 AIAA–2002–0827

Rayleigh Scattering Diagnostic for Measurement of Velocity and Density Fluctuation Spectra

Richard G. Seasholtz
Glenn Research Center, Cleveland, Ohio

Jayanta Panda
Ohio Aerospace Institute, Brook Park, Ohio

Kristie A. Elam
Akima Corporation, Cleveland, Ohio

Prepared for the
40th Aerospace Sciences Meeting and Exhibit
sponsored by the American Institute of Aeronautics and Astronautics
Reno, Nevada, January 14–17, 2002

National Aeronautics and
Space Administration

Glenn Research Center

April 2002

Available from

NASA Center for Aerospace Information
7121 Standard Drive
Hanover, MD 21076

National Technical Information Service
5285 Port Royal Road
Springfield, VA 22100

Available electronically at http://gltrs.grc.nasa.gov/GLTRS

RAYLEIGH SCATTERING DIAGNOSTIC FOR MEASUREMENT OF VELOCITY AND DENSITY FLUCTUATION SPECTRA

Richard G. Seasholtz*
National Aeronautics and Space Administration
Glenn Research Center
Cleveland, Ohio 44135

Jayanta Panda†
Ohio Aerospace Institute
Brook Park, Ohio 44142

Kristie A. Elam‡
Akima Corporation
Fairview Park, Ohio 44126

ABSTRACT

A new molecular Rayleigh scattering based flow diagnostic is used for the first time to measure the power spectrum of gas density and radial velocity component in the plumes of high speed jets. The technique is based on analyzing the Rayleigh scattered light with a Fabry-Perot interferometer used in the static, imaging mode. The PC based data acquisition system is capable of simultaneous sampling of velocity and density at rates to 100 kHz and data record lengths to 10 million. Velocity and density power spectra and velocity-density cross spectra are presented for a subsonic jet, an underexpanded screeching jet, and for Mach 1.4 and Mach 1.8 supersonic jets. Software and hardware interfaces were developed to allow computer control of all aspects of the experiment and data acquisition.

INTRODUCTION

In this paper we describe the initial application of a new flow diagnostic technique for simultaneous measurement of dynamic flow velocity and density based on the molecular Rayleigh scattering of laser light. The objective of the work is to develop an unseeded, nonintrusive dynamic measurement technique for the study of turbulent flows in NASA test facilities. This technique provides aerothermodynamic data not presently obtainable. It is particularly important for supersonic flows where hot wire and pitot probes are difficult to use and which disturb the flow under study. The effort is part of the non-intrusive instrumentation development program supporting propulsion research at the NASA Glenn Research Center. In particular, this work is directed to the measurement of fluctuations in flow velocity, density, and temperature for jet noise studies. These data will be valuable to researchers studying the correlation of fluctuations in flow parameters with far field noise[1]. One of the main objectives in jet noise research is to identify noise sources in the jet and to determine their contribution to noise generation.

A variety of nonintrusive, laser based flow diagnostics (Rayleigh scattering, LDV, PIV, LIF) are routinely applied for time average and instantaneous planar measurements of velocity, density, temperature, and species concentrations. However, an important class of measurements is not addressed by current laser diagnostics. High frequency response dynamic measurements of flow parameters cannot be made with existing techniques. This type of time history data is needed to determine, for example, density and velocity spectra, velocity-density correlations, and two-point correlations. Although Laser Doppler velocimetry (LDV) can typically achieve data rates of a few tens of kHz, it is difficult to achieve much higher rates without introducing larger amounts of seed material into the flow. In practice, LDV normally provides mean velocity and a measure of turbulence intensity. Furthermore, the measurements are random in time, which makes it difficult to obtain time history data needed for power spectra. In turbulent flows, LDV measurements are beset by a variety of so called biasing errors, caused by correlations between the measurement rate and flow properties.

Planar techniques, such as PIV and planar Rayleigh scattering, provide a large number of simultaneous measurements in the measurement plane, but are generally limited to low sampling rates, which are

* Senior Research Engineer
† Senior Research Associate, Member AIAA
‡ Optics Technologist

determined by the pulse repetition rate of the laser and by the time needed to transfer image data from the camera. New techniques are needed to provide nonintrusive, dynamic measurements that can provide data similar to that provided by hot wire anemometers. Since it is unrealistic to expect (at least at the present time) to make measurements simultaneously at a large number of locations and at a high sampling rate, we developed a laser diagnostic capable of single point measurements at a high sampling rate (to 100 kHz).

Another consideration is that LDV and PIV require the flow to be "seeded" with micron seed particles to provide a sufficient concentration of scattering centers. The reliance on seed particles presents a number of problems. To begin with, it is difficult to inject a uniform cloud of seed in many test facilities. Also, because the seed material must withstand the flow environment, refractory materials are necessary for high temperatures. In addition, seed material can contaminate the facility by coating surfaces and windows. Thus, facility engineers are often wary of the introduction of this foreign, often abrasive material, into their equipment. A further limitation of particle scattering methods is that the particles, although small, may not be able to follow large flow accelerations, thereby introducing inaccuracy in the prediction of the gas velocity.

These problems associated with particle scattering measurements are eliminated if molecular scattering is used, since the gas molecules that constitute the flow under study are used as the scattering centers. The simplest molecular scattering based diagnostic is Rayleigh scattering. The frequency spectrum of Rayleigh scattering is closely related to the velocity distribution of the scattering gas, and its characteristics may be used to determine the gas temperature, density, and velocity. Density is simply proportional to the total scattered light; temperature is obtained from the width of the Rayleigh spectrum; and one component of velocity is proportional to the shift of the frequency of the spectra peak from the frequency of the incident light. Because the width is also a function of the molecular weight of the gases in the flow, knowledge of the gas composition is generally required; however, this is not a concern in the proposed work, which is directed toward air flows where the composition is well defined. On the other hand, because velocity is determined from the frequency of the spectral peak, it is independent of the gas composition. Rayleigh scattering is particularly suitable for measurement of supersonic and hypersonic velocity where the mean molecular velocity (flow velocity) is larger than the random molecular velocity (temperature). Previously, we developed a dynamic Rayleigh scattering diagnostic to measure dynamic density fluctuations[2,3]. Since the gas density is proportional to the total Rayleigh scattered light, it is relatively easy to measure, although a calibration procedure is required to determine the proportionality constant. In the present work, we address the more difficult problem of dynamic velocity measurements.

The basic problem in the dynamic measurement of velocity involves the determination of the shift of the peak of the Rayleigh scattering spectrum at high sampling rates. The approach used is based on a Fabry-Perot interferometer used in a static imaging mode, with three photomultiplier tubes (PMT's) and photon counting electronics used for signal detection. Preliminary results for this technique were reported previously for measurements taken in a small laboratory free jet[4]. In that work, measurements could only be made in the jet potential core, which had low turbulence levels. Measurements in the mixing regions could not be made because of scattering from dust particles in the room air. The facility used in the present work, however, uses a clean co-flow to eliminate particles in the mixing region.

The PC based data acquisition system is capable of acquiring simultaneous data from the three photon counters along with two analog channels used for acoustic data. Up to 10 million samples can be acquired at sampling rates to 100 kHz. These long data records allow the computation of power spectra and cross power spectra of gas density, velocity, and far field acoustic data. In this paper we only present results for the flow density and velocity power spectra and velocity-density cross spectra. Results of the acoustic measurements and their correlations with the flow measurements will be presented in a later paper.

We will first briefly present some background on the use of molecular Rayleigh scattering for flow diagnostics. A description of the optical setup and free jet facility will then be given, followed by the results obtained in subsonic flow, in an underexpanded screeching jet, and in Mach 1.4 and Mach 1.8 flow from a converging-diverging nozzle.

THEORY

Rayleigh scattering

The spectrum for Rayleigh scattering from a low density gas (fig. 1) has a Gaussian profile given by

$$S_R(f-f_o)=\frac{2\sqrt{\pi}}{aK}\exp\left\{-\left[\frac{2\pi(f-f_o)-\mathbf{K}\cdot\mathbf{u}}{aK}\right]^2\right\}df \qquad (1)$$

where f_o is the laser frequency and $\mathbf{u}$ is the mean gas velocity. The interaction wave vector is $\mathbf{K} = \mathbf{k}_s - \mathbf{k}_o$ (with $\mathbf{k}_o$ and $\mathbf{k}_s$ being the wave vectors of the incident and scattered light), and $a = (2\kappa T/m)^{1/2}$ is the most probable molecular speed (with κ being Boltzmann's constant, m the molecular mass, and T the gas temperature). Note

that the spectral peak is shifted by a frequency proportional to the component of the bulk velocity in the **K** direction, while the spectral width is proportional to the square root of the gas temperature. It is convenient to introduce the velocity component $u_K = \mathbf{K}\cdot\mathbf{u}/K$, which represents the measured velocity component.

The assumption of a Gaussian shaped Rayleigh scattering spectrum is only valid if

$$y = \frac{p}{\eta K a} << 1$$

where p is the gas pressure and η is the shear viscosity. Collective effects of the molecular motions become important for higher density gases ($y \sim 1$) and a more detailed kinetic theory model, such as the Tenti S6 model[5], is required to describe the Rayleigh scattering spectrum. Although the Tenti spectrum does differ significantly from a Gaussian spectrum for the flows we are studying, similar results are obtained for the uncertainty analysis we conducted. We, therefore, used the Gaussian spectral model to reduce the computational time.

Measurement uncertainty

Since Rayleigh scattering is a relatively weak process, the uncertainty in the measurements is usually set by the photon statistical noise (shot noise), which determines the lower bound on measurement uncertainty. For example, the variance in the number of photoelectron counts for a Poisson process is equal to the mean number of counts. Thus the lower bound for the relative uncertainty in the measurement of gas density ρ, is equal to the square root of the variance divided by the mean counts N_R. The lower bounds for temperature and velocity uncertainties have also been evaluated for a low-density, one-component gas. The relative uncertainties caused by photon statistics for this case can be written [6,7].

$$\frac{\sigma(\rho)}{\rho} = \left(\frac{1}{N_R}\right)^{1/2}, \quad \frac{\sigma(T)}{T} = \left(\frac{2}{N_R}\right)^{1/2}, \quad \sigma(u_K) = \frac{a}{(2N_R)^{1/2}} \qquad (2)$$

These relations provide a lower bound for the measurement uncertainties, which can only be attained if the shot noise is the dominant noise and if an ideal instrument is used.

Consider an experiment with the following parameters: a laser (532 nm) with output power P_o = 5 W, air at STP (T = 293 K, p = 1 atm), probe volume length L_x = 1 mm, f/4 collecting optics (i.e., solid collection angle Ω = 0.05 sr), and efficiency factor ε = 5%. The rate of detected photons, given by

$$N_R = \frac{\varepsilon P_o n L_x \lambda \Omega}{hc}\left(\frac{d\sigma}{d\Omega}\right)\sin^2\chi \qquad (3)$$
$$= 50 \quad \text{million counts/sec}$$

In this equation, n is the gas number density, $d\sigma/d\Omega$ is the differential scattering cross section ($6.13\text{x}10^{-32}$ m^2/sr for air at 532 nm), χ is the angle between the electric field vector of the (linearly polarized) incident light and the direction of the scattered light, h is Planck's constant, and c is the velocity of light. If we wish to obtain independent measurements at a 100 kHz rate, the total number of detectable photons in each period would be 500. Equation 2 (for an ideal instrument) gives the lower bound for measurement of density, temperature and velocity for each 10 μsec period

$$\frac{\sigma(\rho)}{\rho} = 4.5\%, \quad \frac{\sigma(T)}{T} = 6.3\%, \quad \sigma(u_K) = 13\ \text{m/sec}$$

This shows that high sampling rate Rayleigh scattering measurements are at least feasible. It must be emphasized, however, that these values represent the best possible measurements given an ideal instrument. In practice, we are limited to instruments such as the Fabry-Perot interferometer used here, which result in significantly higher uncertainties, as described below. An analysis of the measurement uncertainty for the velocity based on the calculation of the Cramer-Rao lower bound is given in reference 4. That analysis shows that, for the Fabry-Perot interferometer based system used in this work, the measurement uncertainties for velocity is about a factor of six larger than for the ideal instrument (i.e., $\sigma(u_K) \cong 50$ m/sec). This large uncertainty for a single measurement obtained in a 10 μsec time interval means we cannot expect to measure velocity time history with a reasonable accuracy (at least for flow velocities lower than 1000 m/sec.). Fortunately, we are only looking for statistical data. Specifically, we want to measure the power spectrum of flow velocity fluctuations, along with cross power spectra of velocity and density. This allows us to acquire long time history data records, which can be numerically processed to obtain power spectra with reasonable uncertainties.

Fabry-Perot Interferometer

A planar mirror Fabry-Perot interferometer (fig. 2) was used in this work. The instrument function (transmission of a single frequency source) is[8]

$$I_{FP}(\psi) = \left[1 + F\sin^2\left(\frac{\psi}{2}\right)\right]^{-1} \qquad (4)$$

with ψ being the phase change (neglecting any phase change on reflection) of the light between successive reflections given by

$$\psi(f,\theta_r) = \frac{4\pi f \mu d \cos\theta_r}{c} \quad (5)$$

Here, μ is the refractive index of the medium in the Fabry-Perot cavity, d is the Fabry-Perot mirror spacing, θ_r is the angle between the ray and the optic axis, $f = \lambda/c$ is the optical frequency, and $F=1/(\sin^2(\pi/2N_E))$ where N_E is the effective finesse. In general, the image of a monochromatic extended source located in the object plane consists of a series of unequally spaced concentric rings. With a single frequency source, the fringe is relatively narrow. In this work, however, the field of view is restricted by the diameter of the optical fiber and includes only the inner fringe as shown in figure 3.

It is convenient to describe the fringe location in terms of the fringe order rather than fringe radius because of the nonlinear nature of the spectral response of the Fabry-Perot. For example, if there is a bright fringe on axis, concentric bright fringes occur at integral values of lower orders, but the change in fringe radius decreases with decreasing fringe order.

Here we define the fractional order of the fringe with radius r as

$$n = \frac{d}{\lambda}\left(\frac{r}{f_L}\right)^2 \quad (6)$$

where f_L is the focal length of the fringe forming lens. For example, at the location of the image dissector described below in the Optical configuration section, the fringe order of the 6 mm diameter mirror is 0.035. Likewise, the fringe order corresponding to the diameter of the image of the optical fiber is 0.213. So, if unshifted laser light generates a bright fringe with radius r_o, we refer to this as order n_o. Note that here we are using the term "fringe order" to denote change of the fringe order from the actual fringe order on the optical axis, which is $2d/\lambda$.

The change in fringe order with optical frequency is

$$\Delta n = \frac{\Delta f}{FSR} \quad (7)$$

so the change of fringe order Δn with change of velocity ΔV is given by

$$\Delta n = \frac{(2/\lambda)\sin(\theta_s/2)}{FSR}\Delta V \quad (8)$$

where θ_s is the scattering angle. For our setup (θ_s = 90°, FSR = 9.6 GHz) a velocity of 100 m/sec will cause a change in the fringe order Δn = 0.0277.

EXPERIMENT

Facility Description

Experiments were performed in a NASA Glenn facility shown in figure 4. Three different nozzles with 25.4 mm exit diameters were used. One nozzle was a convergent design, which was used for subsonic flow measurements and to produce a screeching underexpanded jet with fully expanded Mach number 1.42. The other nozzles (Mach 1.4 and 1.8) were convergent-divergent types designed by the method of characteristics. (Design details are given in reference 9.) The supply air was unheated with an average total temperature of 297 K, which was also the average ambient temperature. The average air density was 1.17 kg/m^3. The facility was located in a large test chamber with acoustic absorbent material placed around the vicinity of the nozzle and on the ceiling and walls of the test cell to minimize reflections. The optics were mounted on a remotely controlled traversing system that allowed flow measurements to be made in the horizontal x-y plane. Wherever possible, various parts of the optical train, air supply duct and jet facility were covered with 1/4 inch thick polyurethane foam to further reduce acoustic reflections.

A critical requirement in the use of molecular Rayleigh scattering for flow diagnostics is a clean, particle-free air flow. The primary air supply to the jet was filtered to remove particles. In addition, a 200 mm diameter low-velocity filtered co-flow surrounded the jet. This co-flow was generated by an air handling system that filtered the ambient air. The primary air supply was dried to a 230 K dew point, which was sufficient to prevent condensation in the core flow for all flow conditions. However, condensation did occur in the mixing regions of the jet for the Mach 1.8 supersonic flow when the facility was started. This difficulty was eliminated by running the jet for an hour or two to reduce the ambient air humidity to a level where condensation did not occur.

Optical configuration

Light from a 5W, 532 nm, diode-pumped solid-state (DPSS), single-frequency, Nd Vanadate CW laser was focused by a 350 mm focal length lens (L1) to a 150 μm diameter beam at the probe volume on the nozzle centerline (fig. 5a). This beam is in the horizontal direction, perpendicular to the flow axis, and is terminated in a light trap. Rayleigh scattered light is collected in the vertical direction at a 90° scattering angle and focused by a pair of lenses (L2) (f/4.7, 300 mm focal length and f/2, 160 mm focal length) into a 0.55 mm core diameter multimode optical fiber. The effective length of the probe volume (defined by the

fiber diameter and the collection lenses) is 1.0 mm. The laser was mounted in an acoustic enclosure with vibration isolation mounts to minimize the amount of laser frequency modulation caused by vibration of the laser head. Additional optics provided a reference image of light at the unshifted laser frequency. To accomplish this, remotely controlled pneumatic actuators placed a mirror (M) and a diffuser (D) in the optical path. When in the beam path, the mirror directed laser light onto the diffuser, which scattered light into the optical fiber.

The fiber was routed from the high acoustic level environment of the jet to a quiet, remote area where the detection optics were located. Figure 5b shows the layout of the optics and Fabry-Perot interferometer that make up the detection system to measure the flow velocity. The light exiting the fiber is collimated by lens L3 (100 mm focal length) and split into two paths with an uncoated optical flat (BS1). About 10% of the light is reflected and focused by lens L4 (f/2, 160 mm focal length) onto PMT 1 (quantum efficiency ~ 25 %). This signal is proportional to gas density. The light transmitted by the beamsplitter is directed through a planar mirror Fabry-Perot interferometer (70 mm dia. mirrors, 90% reflectivity, 10 GHz free spectral range (FSR), finesse ~ 15). The light exiting the interferometer is focused by the fringe-forming lens, L6. This lens consists of a pair of 35-mm camera lenses (f/4, 300 mm focal length and f/2.8, 60 mm focal length) that are spaced to give an effective focal length of 2727 mm. This forms a 15 mm diameter image of the fiber core at the focus of the interferometer fringes. Because of the limited size of the fiber, only a single circular fringe is formed (fig. 6). At the focal plane of the fringe pattern, the light is divided into two parts by a pair of mirrors (image dissector). A small mirror (6 mm dia.) is centered on the fringe pattern and directs light from the inner part of the fringe through lens L7 (f/4, 200 mm focal length) to PMT 2. This small mirror is mounted on a larger mirror (25 mm dia.) that directs light from the outer part of the fringe through L8 (f/4, 200 mm focal length) to PMT 3. The mirrors are tilted ± 3° with respect to the optical axis. A typical image of the inner fringe of Rayleigh scattered light is shown in figure 6a. Note that a flow in the direction of the **K** vector, which here is in the radial direction (fig. 5a), results in a positive frequency shift and increasing fringe diameter, while a flow in the direction opposite the **K** vector results in a negative frequency shift and decreasing fringe diameter. Thus, as the frequency of the Rayleigh scattered light increases, less light is detected by PMT 2 (inner) and more light is detected by PMT 3 (outer).

Expected photoelectron count rates

The approximate total detectable photon collection rate for this optical configuration, as given by equation 3, is N_R = 50 million counts/sec.

The expected number of photons detected in time interval Δt by detector 1 (PMT 1) is $R_B N_R \Delta t$ where R_B is the reflectivity of the beamsplitter BS. The expected number of photons detected by PMT 2 and PMT 3 are

$$\langle N_{Dq} \rangle = (1-R_B) N_R \Delta t \iint S_R(f) I_{FP}(f, \theta_r)\, df\, dA \quad (9)$$

where $S_R(f)$ is the Rayleigh scattering spectrum given by equation 1. The integrations are over frequency and the area of the q^{th} detector (i.e., PMT 2 or 3), and I_{FP} is the Fabry-Perot instrument function given by equation 4.

Software

The data acquisition system was completely automated by two Labview programs. One maintained the fringe radii by controlling the interferometer PZT's, while the second acquired the data. These programs worked in conjunction with each other.

Fringe stabilization

The stabilization program began by sending a signal over a DAQ board's digital lines to place a prism assembly (PA on fig. 5b) into the light path between the interferometer and the fringe-forming lens. This divided the light into three images which were sent to a standard video camera and digitized by a PC frame grabber card. The radii were measured by first taking horizontal and vertical cross-sections of +/- 65 pixels from the fringe centers. These values were fed into a nonlinear Levenberg-Marquardt routine that fit the fringe profiles to a model of the Fabry-Perot instrument (eq. 4). The average of the radii obtained from the horizontal and vertical cross-sections for each fringe were processed by a Fuzzy Logic algorithm to generate correction signals. These signals were output using a D/A board, amplified using an external high voltage amplifier, and applied to the Fabry-Perot PZT's to adjust the mirror alignment. When the current radii matched the target radius within a certain limit, "locked" status was achieved. Once this occurred, the program would maintain these radii. If the interferometer were to drift and the fringe radii change, the feedback loop would adjust the PZT values until the status was again locked. As the program ran, a continuous history of the fringe radii and interferometer PZT values was saved to a data file for later study.

Data Acquisition

Once the required fringe radius was achieved and maintained, the data acquisition program set the stabilization program into 'sleep' status, in which the feedback loop was disabled. Using the digital lines on a DAQ board, the three PMT high voltages were turned on, the diffuser was placed into the beam path, and the PA was removed from the beam path to send light to the inner and outer fringe PMT's. Photoelectron pulses from the three PMT's were amplified (gain = 5) and sent to constant fraction discriminators (CFD). The CFD's output 10 ns wide TTL level pulses that were counted by a PC counter-timer board configured for three channels corresponding to the inner and outer fringe areas, and the total density. Data was acquired simultaneously on the three channels at rates to 100 kHz. In addition, one or two analog channels (used for microphone signals) were digitized with an A/D board simultaneously with the counter data. To achieve synchronization between the four or five channels, the A/D board was connected to the counter board via a RTSI cable. The channels were first armed, and then a finite pulse train at the given sampling rate was generated on the counter-timer board. Typical photoelectron count rates were on the order of 5 MHz. The accumulated counts on each channel were recorded at time intervals of 100 μsec, while the number of counts in each time interval was given by the difference between adjacent values of the accumulated counts. These data were recorded to a binary file. Total pressure and temperature of the interferometer were recorded using an IEEE interface. Mean and variance of the time interval counts were also calculated. When data acquisition was complete, the PA was moved back into the light path, and the fringe radii were again stabilized.

Data processing

The photon counter data were first adjusted to compensate for pulse pileup errors. For a photon counter with pulse resolution time τ and bin width ΔT, the measured number of counts N_M is related to the true number of counts N_T by

$$N_M = N_T e^{-N_T\left(\frac{\tau}{\Delta T}\right)} \tag{10}$$

solving for N_T gives the approximate correction

$$N_T = \frac{2}{1+\sqrt{1-4N_M\left(\frac{\tau}{\Delta T}\right)}} N_M \tag{11}$$

Note that the observed count rate is $N_M/\Delta T$. The highest photoelectron count observed in our measurements was about 5 million counts/sec. For our photon counting system, with a pulse resolution time of 10 nsec, the maximum correction was about 10%.

The gas density was obtained in a straightforward manner, since it is proportional to the total Rayleigh scattered light measured by PMT 1. Calibration constants (slope and intercept) were found using a linear least squares fit of the PMT 1 counts as a function of the gas density (obtained using the calibration jet).

For the velocity calibration, an operating region was selected such that the count rate for the inner and outer regions was approximately linear with respect to velocity. Data were taken using a calibration jet with the flow axis aligned in the radial direction of the main jet. The calibration velocity was calculated from the total temperature and pressure ratio using isentropic flow relations. A linear fit of the inner (I) and outer counts (O) as a function of velocity was then done to obtain the four constants A_1, B_1, A_2, and B_2.

$$I = A_1 + B_1 V, \quad O = A_2 + B_2 V \tag{12}$$

These were solved to find the velocity as a function of the ratio $R = O/I$.

$$V = \frac{A_2 - A_1 R}{B_1 R - B_2} \tag{13}$$

This rational function of $V = V(R)$ could also have been obtained by directly doing a nonlinear fit, but this would have required an iterative algorithm. Because the velocity is only a function of the ratio of the outer and inner counts, it is independent of the any change in the total scattered light level. Additional details on the calibration procedure are given in reference 4.

After the calibration constants were obtained, the dynamic data were processed by applying equation 13 for each data point to obtain a velocity time history record. Because of the relatively high level of shot noise (typically, each time interval had about 100 counts), the time history exhibited fluctuations on the order of the velocity fluctuations. However, by using long data records, the power spectrum of the velocity fluctuations could be calculated using the technique described in the following section.

Welch method of modified periodograms

We used the Welch method of modified periodograms[10] to calculate an estimate of the velocity fluctuation power spectrum. In this procedure, a long data record sampled at rate f_s for time T (total samples = $N = Tf_s$) is subdivided into a number K_r of smaller

records (which may be overlapping), each of length L samples. The modified periodograms of each sub-record are calculated using a data window; these individual periodograms are then averaged to obtain the estimate of the power spectrum. The frequency resolution of the resulting spectrum is thus f_s/L. By overlapping the segments by one half of their length, a near maximum reduction in the variance in the spectral estimate is achieved; the variance in the estimated spectrum is reduced by a factor of $11/9K_r$ compared to the variance of the spectral estimate calculated directly from the original long data record. We used a sub-record length L = 1024 for all our data, giving a frequency resolution of $f_s/1024$.

We present our results as one-sided power spectral density (PSD) plots[11]. In general, for two data records $x(t)$ and $y(t)$, the cross power spectral density is written

$$G_{xy}(f) = C_{xy}(f) - iQ_{xy}(f) \tag{14}$$

where the real part C_{xy} is the coincident spectral density and the imaginary part Q_{xy} is the quadrature spectral density. For $x(t)$ equal $y(t)$, this reduces to the autospectral density $G_{xx}(f)$, which we will just refer to as power spectral density. The power spectral density is normalized so that the integral of $G_{xx}(f)$ over the frequency range $[0,f_c]$ is equal to the variance of the data, i.e.

$$\int_0^{f_c} G_{xx}(f)df = \left\langle \left(x(t) - \langle x(t) \rangle \right)^2 \right\rangle \equiv \sigma_x^2 \tag{15}$$

where f_c is the Nyquist frequency (half the sampling rate).

The power spectral density for our measurements can be thought of as the result of a doubly stochastic process[12] with the measured PSD $G_{M,xx}(f)$ having two components

$$G_{M,xx}(f) = G_{T,xx}(f) + G_{S,xx}(f) \tag{16}$$

where $G_{T,xx}(f)$ is due to the turbulent flow fluctuations and $G_{S,xx}(f)$ is due to the photon statistical noise (shot-noise). Because the shot-noise has Poisson statistics, the variance of the number of counts is equal to the mean number of counts. The power spectral density of the shot noise is constant[13] (i.e., white noise) with a value equal σ_S^2 / f_c. We subtract this shot-noise contribution from the measured spectrum, which should leave only the contribution from the turbulent flow fluctuations. (Although, as shown in the results section, this doesn't work exactly as theory predicts.)

The cross power spectral density $G_{xy}(f)$ can be expressed in terms of coherence $\gamma_{xy}(f)$ and phase $\theta_{xy}(f)$

$$\gamma^2_{xy}(f) = \frac{|G_{xy}(f)|^2}{G_{xx}(f)G_{yy}(f)}$$
$$\theta_{xy}(f) = \tan^{-1}\left(\frac{Q_{xy}(f)}{C_{xy}(f)} \right) \tag{17}$$

where the shot noise base is subtracted from $G_{xx}(f)$ and $G_{yy}(f)$ in the expression for coherence.

Another consideration in measuring the power spectrum is the sampling rate, which should be at least twice the maximum frequency of the turbulent fluctuations. The usual practice in acquiring dynamic data is to use a sharp cutoff lowpass filter with the cutoff frequency at the Nyquist frequency. However, photon counting, which is an "integrate and dump" process, results in a low pass filter with frequency response

$$H(f) = \frac{2\sin(2\pi f \Delta t/2)}{2\pi f \Delta t} \tag{18}$$

where Δt is the bin width. As shown in figure 7, the response falls off slowly, has only 3dB attenuation at the Nyquist frequency, and falls to zero at the sampling frequency. However, it exhibits significant transmission above the sampling frequency. This means that the turbulence should not have any significant fluctuations at frequencies above the Nyquist frequency, and compensation should be used for frequencies below the Nyquist frequency (although we did not apply this correction to the data presented in this paper). The white shot noise spectrum does undergo aliasing. Interestingly, inclusion of the aliased broadband shot-noise results in a flat spectrum. Because of these factors, the sampling rate for a photon counting system should be greater than the sampling rate one would use in a conventional analog data acquisition system.

EXPERIMENTAL RESULTS

Calibration

The first step was to obtain calibration data using a small subsonic free jet aligned along the **K** direction (the radial direction of the facility jet). This total temperature and pressure were measured and were used to calculate the velocity and density using the isentropic flow relations. Because we are only measuring the radial flow component, flow velocities up to about 160 m/sec were used. Calibration data were only taken for flow in one direction, outward from the axis of the facility jet. It was assumed that the calibration obtained using the technique described in the data processing section was also valid for flow in the opposite direction. As a check, the velocity probability distribution was

examined. It was very close to Gaussian, which is expected for the velocity fluctuations. One factor that affected the calibration was that the actual fringe radius varied from the setpoint radius (target radius) by as much as 0.5 pixels, which resulted in varying DC offsets. Because spectral measurements were the objective of this work, DC offsets in the calibration were not considered significant.

Converging nozzle

Data was taken in a Mach 0.6 subsonic flow and compared with hot wire data previously taken at the same flow condition. Figure 8 shows the power spectrum of the radial velocity component on the centerline at an axial location X/D = 10. The Rayleigh scattering measurement is shown in figure 8a, where the sampling rate was 20 kHz and the number of samples was 5 million (for a data acquisition time of 250 sec). The power spectrum of the radial velocity component obtained from the X-wire hot wire probe is shown in figure 8b. Although the hot wire probe was sampled at 50 kHz, the spectrum is shown over a 10 kHz range to allow easy comparison with the Rayleigh scattering spectrum. The Rayleigh scattering and hot wire spectra have similar shapes, with a peak at about 1600 Hz. The amplitude of the peak in the Rayleigh scattering spectrum, however, is about a factor two larger than the peak of the hot wire spectrum. This may be due to a possible difference in the probe locations (the data were taken at different times) or to calibration errors. The peak in the velocity spectrum at 430 Hz is caused by vibration-induced frequency modulation of the laser. Figure 9 shows the power spectrum of the density fluctuations and the velocity-density coherence obtained from the Rayleigh scattering measurements. The density power spectrum is relatively flat, as expected for this low Mach number flow. The velocity and density coherence is low. The low frequency peaks in the density spectrum are probably caused by vibration and not by flow fluctuations.

The pressure was increased to a fully expanded Mach 1.42 condition, which generated strong screech tones. Figure 10 shows Rayleigh scattering velocity and density spectral data taken at Y/D = 0.4, X/D = 3. Strong screech tones occur at 4540 Hz and its second harmonic. Also shown in figure 10 is the velocity-density coherence (expressed as γ^2 as given by eq. 17) and the relative phase. This shows that the density and velocity fluctuations are strongly correlated at the fundamental screech frequency. For this data, the sampling rate was 40 kHz and the number of samples was 1 million (acquisition time of 25 sec).

Mach 1.8 Converging-diverging nozzle

Figure 11 shows data taken along the centerline at X/D = 4, 8, and 12 in Mach 1.8 flow. At X/D = 4, the density and radial velocity component have only weak fluctuations, and the coherence is small. At X/D= 8, the velocity and density spectra both shows a peak at about 5000 Hz, but are not strongly correlated.

At X/D = 12, the velocity spectrum has a peak at about 4000 Hz, but the density spectrum does not have a definite peak, with the spectral density increasing toward low frequencies. The density and velocity show relatively strong coherence with a phase difference of about 2.5 radians.

Figure 12 shows data taken along the shear layer (Y/D = 0.48) at X/D = 4, 8, and 12. Strong fluctuations are shown at all these locations. Both the density and velocity spectra have peaks, with the peak frequency decreasing from about 10 kHz at X/D = 4 to less than 5 kHz at X/D = 12. Note that the shape of the density spectrum at X/D = 12 differs from the shape of spectrum along the jet axis. The density and velocity fluctuations are correlated, with a relative phase of about 2 radians. The sampling rate for this nozzle was 40 kHz and the number of samples was 3 million (acquisition time of 75 sec).

Discussion

All the spectral plots show low-frequency components that are not due to flow fluctuations. The low frequencies in the density spectra are probably caused by modulation of the intensity of the light being coupled into the optical fiber as a result of vibrations caused by the high acoustic levels. The velocity spectra show a strong peak at about 450 Hz, which is caused by modulation of the laser frequency due to vibrations coupled in the laser head.

Note that although the shot-noise base was subtracted from the spectrum, the spectral density did not approach zero at high frequencies, as predicted by theory. The reason for this is not known. It could be caused by some high frequency modulation of the scattered light, or it could be caused by some deviation from the assumed ideal Poisson statistics of the light.

The sampling rate was not high enough for some of the flow conditions. This likely resulted in aliasing for these cases. Photon counting prevents the use of a sharp cutoff lowpass filter as is used in analog data acquisition. Higher sampling rates should be used to ensure the flow fluctuations do not have any significant components at frequencies above the Nyquist frequencies.

CONCLUDING REMARKS

The results presented in this paper demonstrate an important new tool for study of turbulent flows, particularly supersonic flows. For the first time, simultaneous measurements of velocity and density fluctuations can be made in supersonic flows. The application of molecular Rayleigh scattering offers a means to determine flow properties by directly measuring the dynamics of the molecules making up the flow. This avoids the issue of flow seeding, with all its attendant problems.

A number of precautions must be exercised, however, in applying this technique. The flow must be free of particles. Long data records must be taken to allow suppression of the high level of shot-noise caused by the weak scattering process. The test facility must be dark to avoid excess background signals. The laser setup must be done carefully to avoid stray scattered light being detected. The laser and optical setup in the test facility must be rugged to minimize extraneous signals caused by vibrations. The extremely sensitive Fabry-Perot interferometer must be located in a quiet location, with the collected Rayleigh scattered being transmitted through an optical fiber.

REFERENCES

[1] Schaffar, M., "Direct measurements of the correlation between axial in-jet velocity fluctuations and far-field noise near the axis of a cold jet", *J. Sound and Vibration*, **64**, pp. 73-83, 1979.

[2] Panda, J., and Seasholtz, R.G., "Measurements of shock structure and shock-vortex interaction in underexpanded jets using Rayleigh scattering", *Phys. Fluids*, **11**, pp. 3761-3777, 1999.

[3] Panda, J. and R.G. Seasholtz, "Investigation of density fluctuations in supersonic free jets and correlation with generated noise", *6th Aeroacoustics Conference*, Lahaina, HI, AIAA-2000-2099, 2000.

[4] Seasholtz, R.G., J. Panda, and K.A. Elam, "Rayleigh scattering diagnostic for dynamic measurement of velocity fluctuations in high speed jets", *AIAA 39th Aerospace Sciences Meeting*, Reno, NV, AIAA-2001-0847, 2001.

[5] Tenti, G., Boley, C.D. and Desai, R.C., "On the kinetic model description of Rayleigh Brillouin scattering from molecular gases", *Can. J. Phys.* **52**, pp. 285-290, 1974.

[6] Seasholtz, R.G., "High-speed anemometry based on spectrally resolved Rayleigh scattering", *Fourth International Conference on Laser Anemometry*, Cleveland, Ohio, 1991 [also NASA TM-104522].

[7] Seasholtz R.G. and Lock, J.A., "Gas temperature and density measurements based on spectrally resolved Rayleigh-Brillouin scattering", *NASA Langley Measurement Technology Conference*, Hampton, VA, 1992.

[8] Vaughan, J.M., *The Fabry Perot Interferometer, History, Theory, Practice and Applications*, Adam Hilger, Bristol, pp. 89-112, 1989.

[9] Panda, J. and Seasholtz, R.G., "Density fluctuation measurement in supersonic fully expanded jets using Rayleigh scattering", 5th *AIAA/CEAS Aeroacoutics Conference*, Seattle ,WA, AIAA-99-1870, 1999.

[10] Welch, P.D., "The use of fast Fourier transform for the estimation of power spectra: A method based on time averaging over short, modified periodograms", *IEEE Trans. on Audio and Electroacoustics*, **AU-15**, pp. 70-73, 1967.

[11] Bendat, J.S., and Piersol, A.G., *Engineering Applications of Correlation and Spectral Analysis*, John Wiley & Sons, New York, pp. 43-56, 1980.

[12] Goodman, J.W., *Statistical Optics*, John Wiley & Sons, New York, pp. 95-97, 1985.

[13] Taub, H., and Schilling, D.L., *Principles of Communication Systems*, McGraw-Hill, New York, pp. 260-263, 1971.

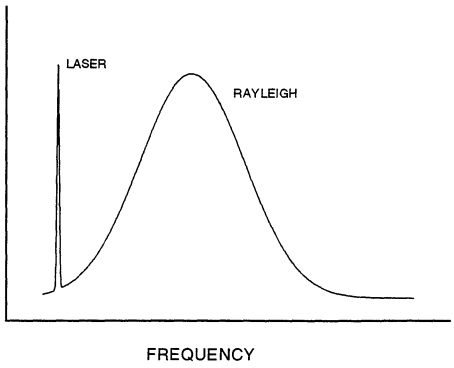

Fig. 1.—Rayleigh scattering spectrum.

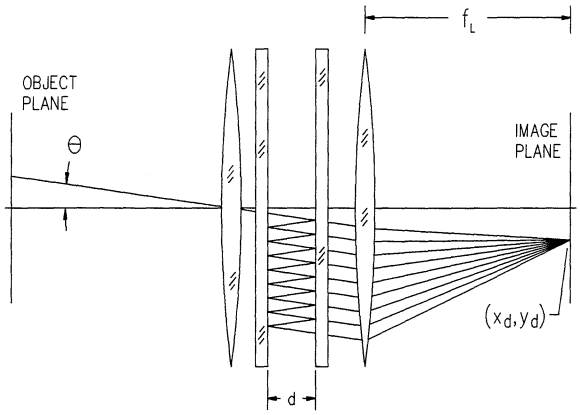

Fig. 2.—Planar mirror Fabry-Perot interferometer.

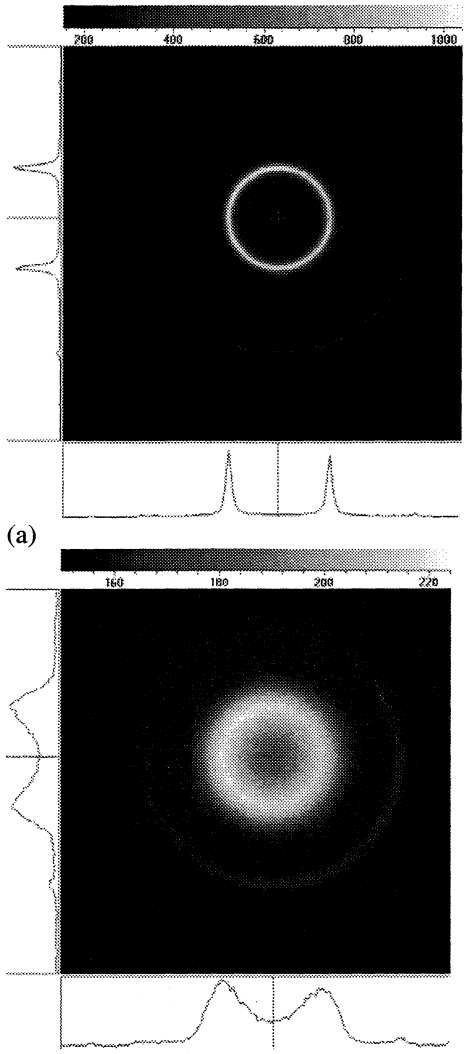

Fig. 3.—Fabry-Perot interferometer images; (a) reference image; (b) Rayleigh scattering image.

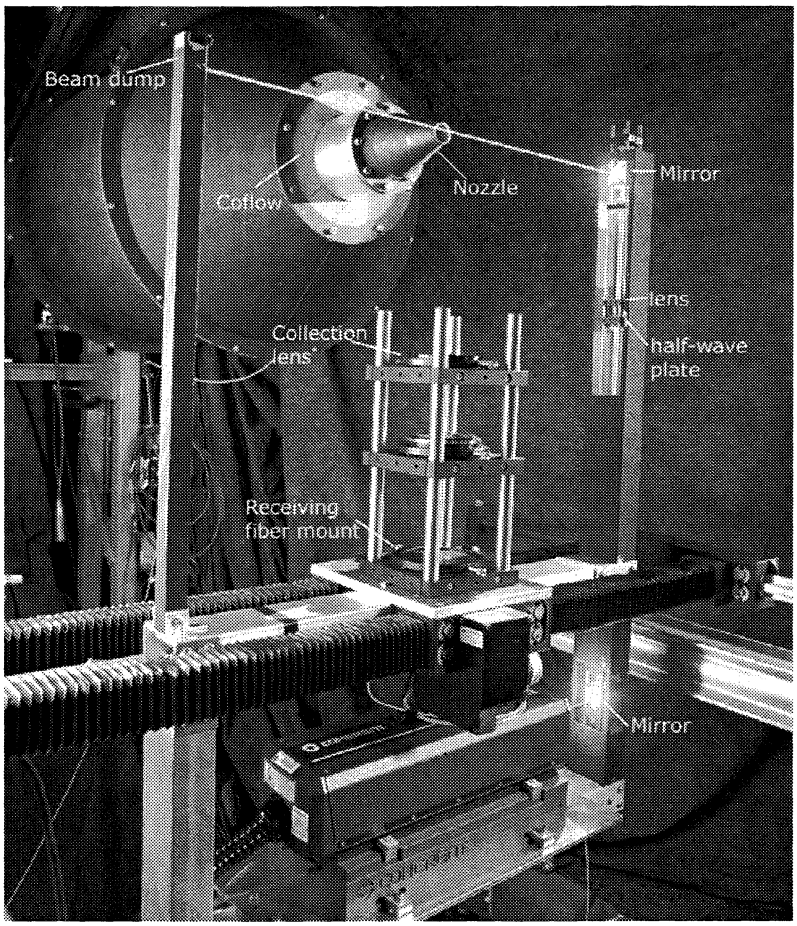

Fig. 4.—Free jet facility showing laser and optics.

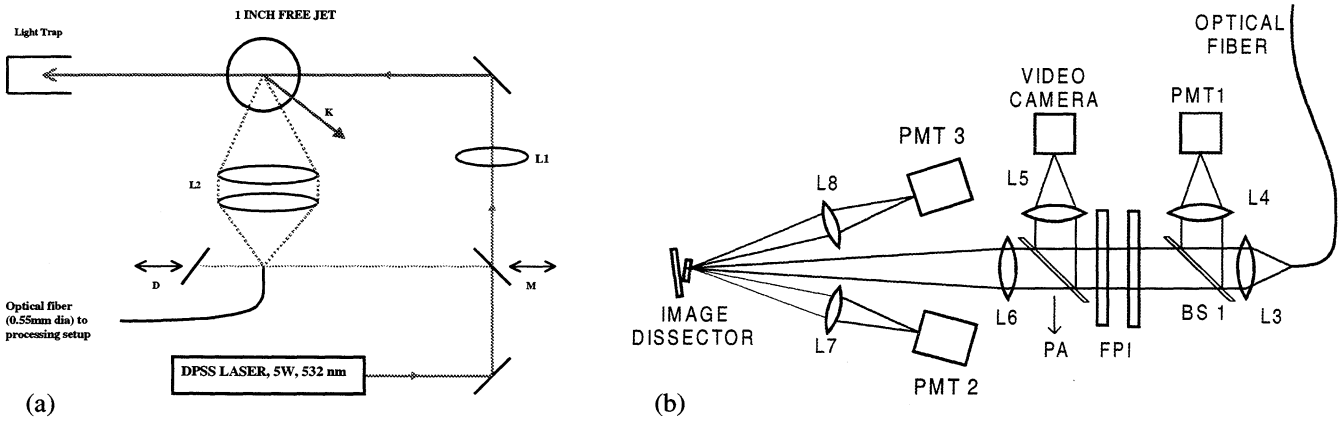

Fig. 5.—(a) Optical setup for free jet facility; (b) Optical processing system for Rayleigh scattering light.

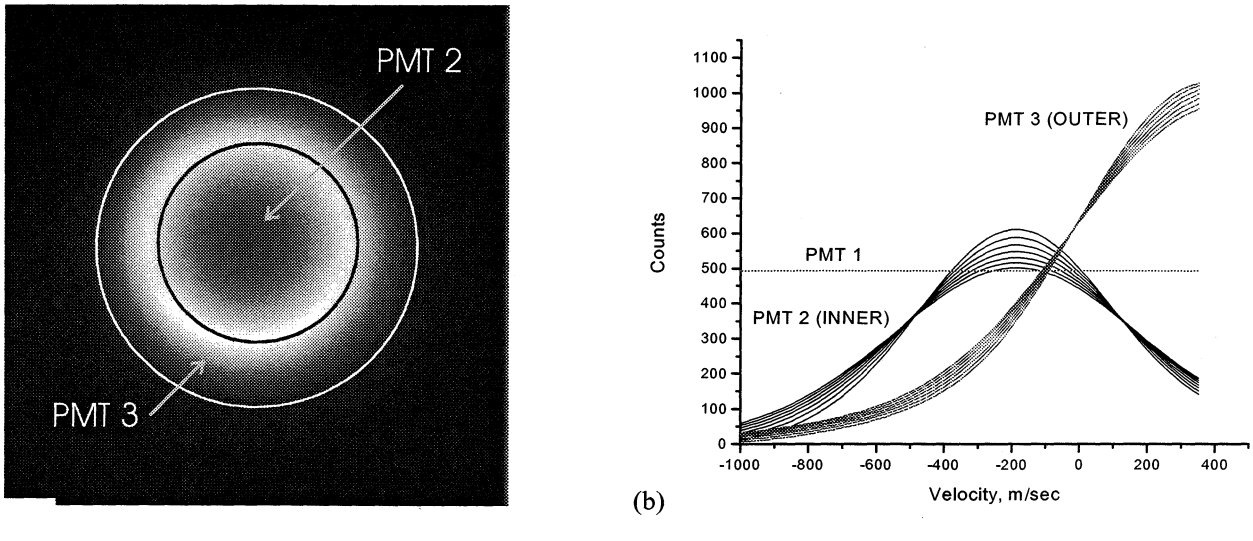

Fig. 6.—(a) Image of fringe formed by Rayleigh scattered light showing regions directed to PMT's 2 and 3; (b) Change of light detected by PMT's as a function of flow velocity along K vector for gas temperatures from 150 to 300 K.

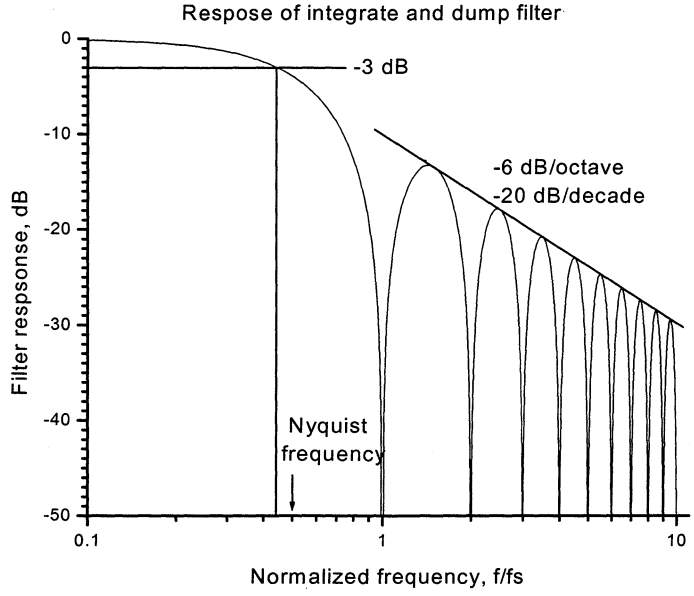

Fig. 7.—Response of light measurement using photon counting signal acquisition procedure ("integrate and dump"). Sampling frequency is f_s.

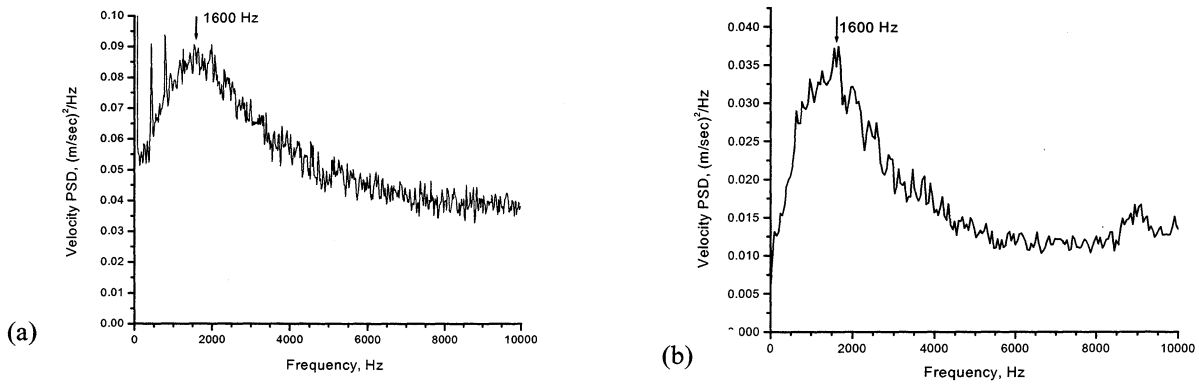

Fig. 8.—Power spectrum of radial velocity component fluctuations on centerline of Mach 0.6 free jet at axial location X/D = 10. (a) from Rayleigh scattering measurements; (b) from hot wire probe.

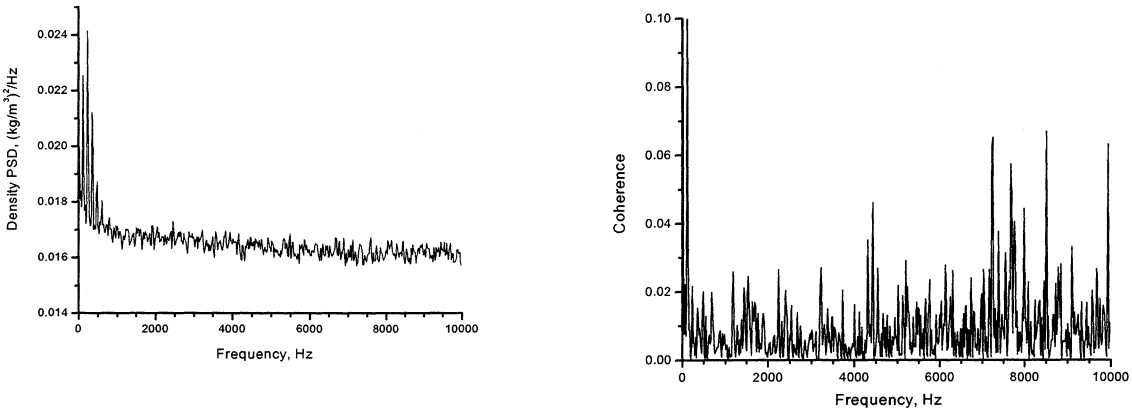

Fig. 9.—Power spectrum of density fluctuation and velocity-density coherence on centerline of Mach 0.6 free jet at axial location X/D = 10.

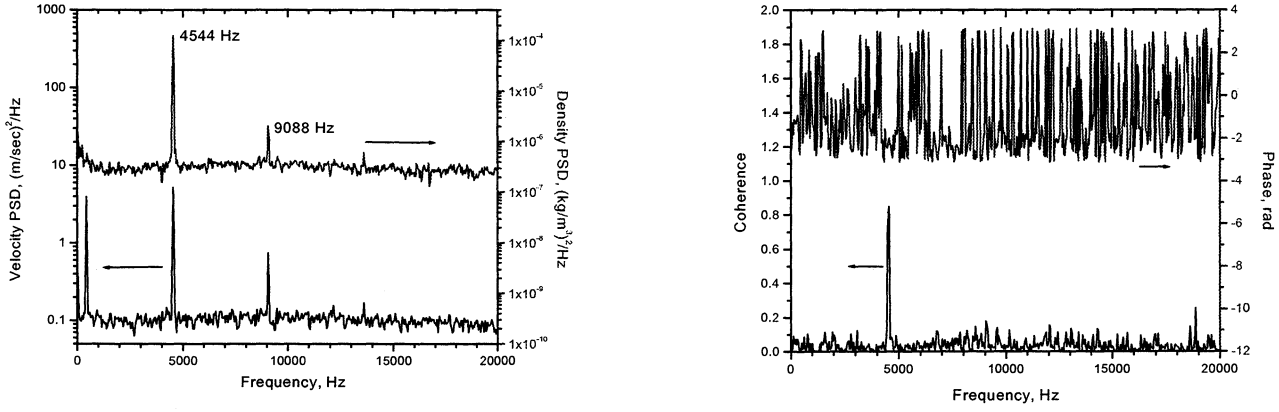

Fig. 10.—Power Spectral Densities of velocity and density (left); and Cross Spectra, coherence (γ^2) and phase (right) of Mach 1.42 underexpanded free jet, X/D = 3, Y/D = 0.4 .

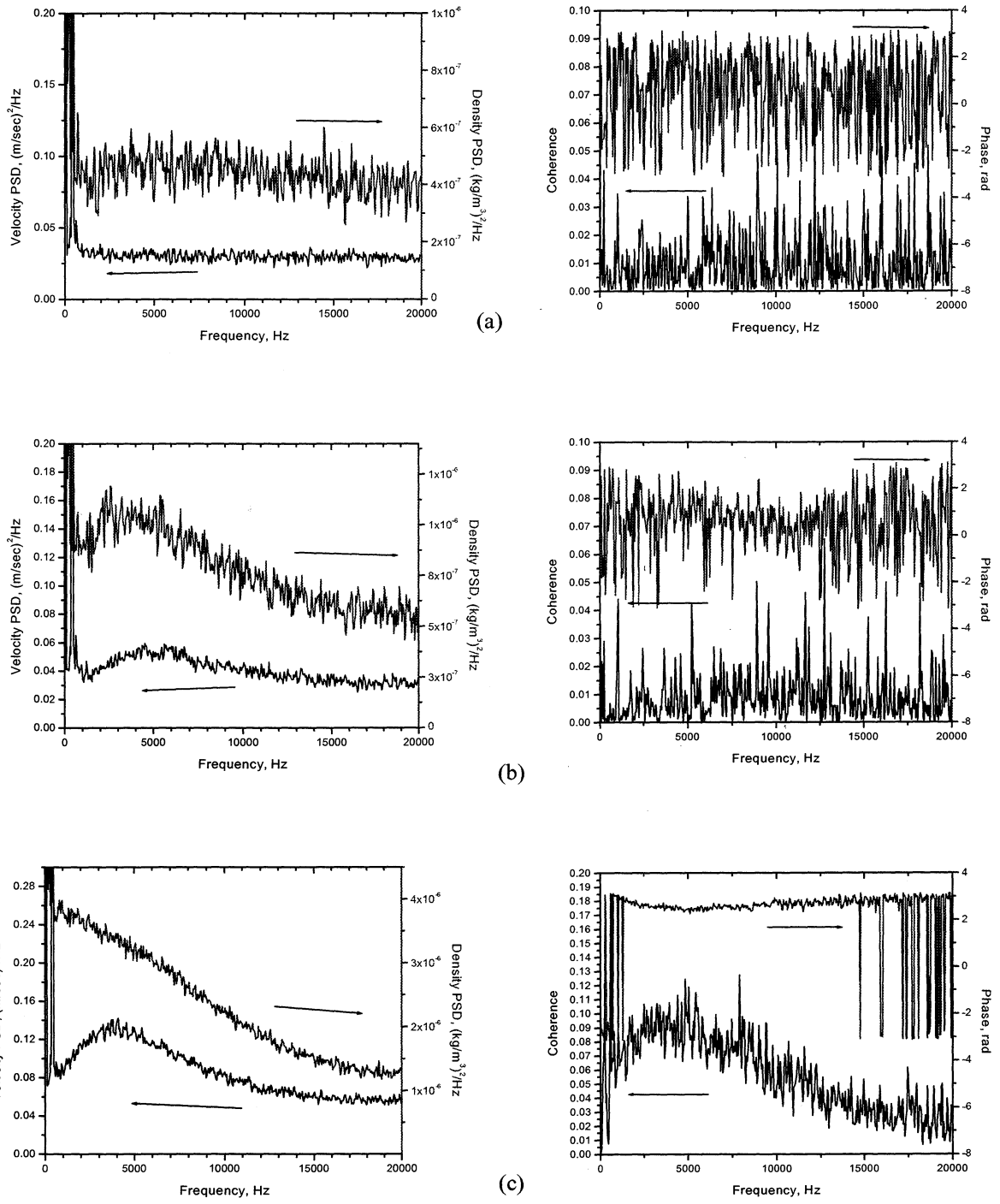

Fig. 11.—Power Spectral Densities of velocity and density (left); and Cross Spectra, coherence (γ^2) and phase (right) on centerline of Mach 1.8 supersonic free jet: (a) X/D = 4; (b) X/D = 8; (c) X/D = 12.

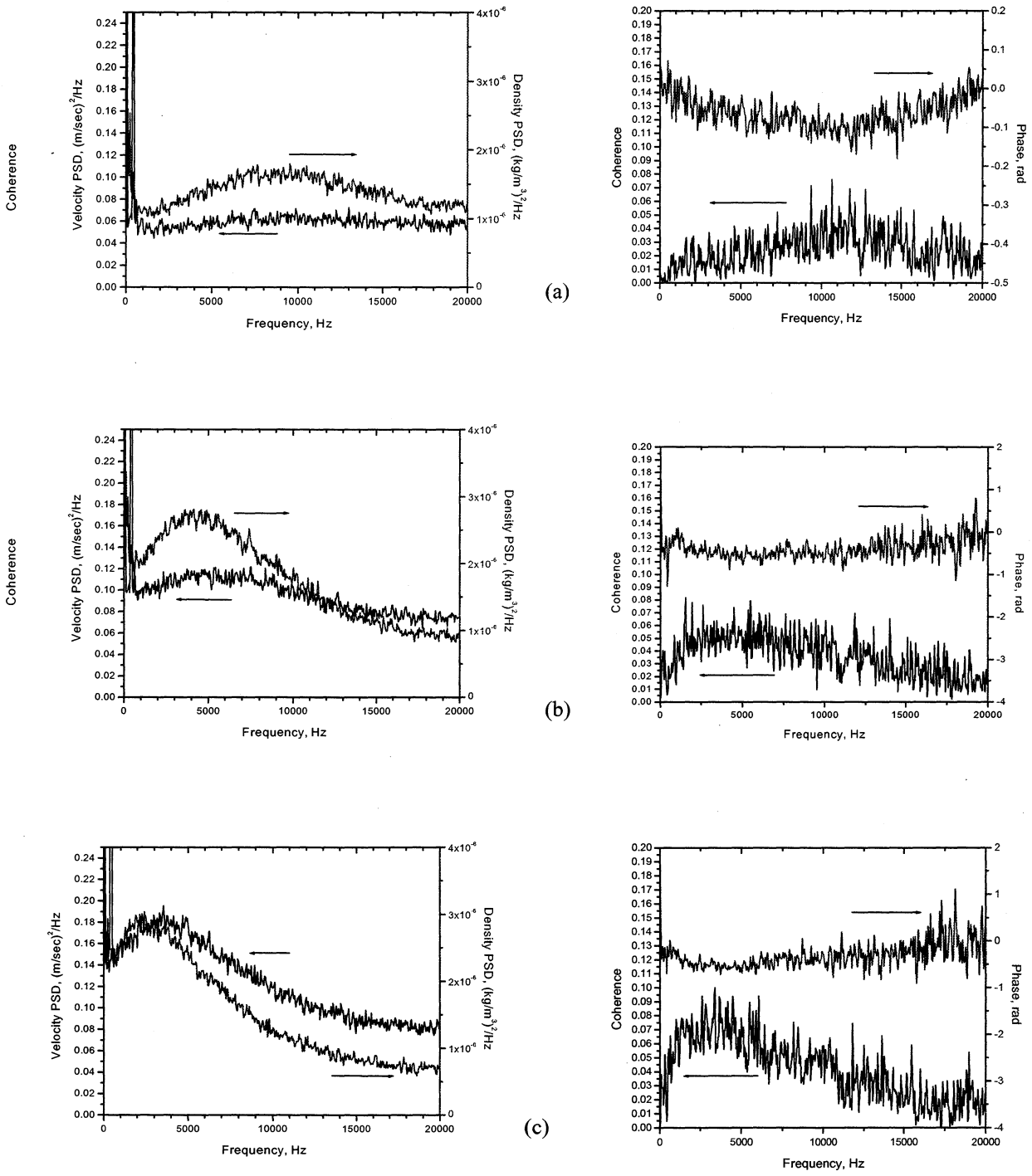

Fig. 12.—Power Spectral Density of velocity and density (left); and Cross Spectra, coherence (γ^2) and phase (right) of Mach 1.8 supersonic free jet along shear layer (Y/D = 0.48): (a) X/D = 4; (b) X/D = 8; (c) X/D = 12.

REPORT DOCUMENTATION PAGE

Form Approved
OMB No. 0704-0188

1. AGENCY USE ONLY (*Leave blank*)	2. REPORT DATE	3. REPORT TYPE AND DATES COVERED
	April 2002	Technical Memorandum

4. TITLE AND SUBTITLE

Rayleigh Scattering Diagnostic for Measurement of Velocity and Density Fluctuation Spectra

5. FUNDING NUMBERS

WU–704–20–13–00

6. AUTHOR(S)

Richard G. Seasholtz, Jayanta Panda, and Kristie A. Elam

7. PERFORMING ORGANIZATION NAME(S) AND ADDRESS(ES)

National Aeronautics and Space Administration
John H. Glenn Research Center at Lewis Field
Cleveland, Ohio 44135–3191

8. PERFORMING ORGANIZATION REPORT NUMBER

E–13270

9. SPONSORING/MONITORING AGENCY NAME(S) AND ADDRESS(ES)

National Aeronautics and Space Administration
Washington, DC 20546–0001

10. SPONSORING/MONITORING AGENCY REPORT NUMBER

NASA TM—2002-211504
AIAA–2002–0827

11. SUPPLEMENTARY NOTES

Prepared for the 40th Aerospace Sciences Meeting and Exhibit sponsored by the American Institute of Aeronautics and Astronautics, Reno, Nevada, January 14–17, 2002. Richard G. Seasholtz, NASA Glenn Research Center; Jayanta Panda, Ohio Aerospace Institute, 22800 Cedar Point Road, Brook Park, Ohio 44142; and Kristie A. Elam, Akima Corporation, Cleveland, Ohio 44135. Responsible person, Richard Seasholtz, organization code 5520, 216–433–3754.

12a. DISTRIBUTION/AVAILABILITY STATEMENT

Unclassified - Unlimited
Subject Category: 35 Distribution: Nonstandard

Available electronically at http://gltrs.grc.nasa.gov/GLTRS

This publication is available from the NASA Center for AeroSpace Information, 301–621–0390.

12b. DISTRIBUTION CODE

13. ABSTRACT ***(Maximum 200 words)***

A new molecular Rayleigh scattering based flow diagnostic is used for the first time to measure the power spectrum of gas density and radial velocity component in the plumes of high speed jets. The technique is based on analyzing the Rayleigh scattered light with a Fabry-Perot interferometer used in the static, imaging mode. The PC based data acquisition system is capable of simultaneous sampling of velocity and density at rates to 100 kHz and data record lengths to 10 million. Velocity and density power spectra and velocity-density cross spectra are presented for a subsonic jet, an underexpanded screeching jet, and for Mach 1.4 and Mach 1.8 supersonic jets. Software and hardware interfaces were developed to allow computer control of all aspects of the experiment and data acquisition.

14. SUBJECT TERMS	15. NUMBER OF PAGES
Rayleigh scattering; Fabry-Perot interferometers	21
	16. PRICE CODE

17. SECURITY CLASSIFICATION OF REPORT	18. SECURITY CLASSIFICATION OF THIS PAGE	19. SECURITY CLASSIFICATION OF ABSTRACT	20. LIMITATION OF ABSTRACT
Unclassified	Unclassified	Unclassified	